PROBABILISTIC TSUNAMI HAZARD ASSESSMENT ALONG THE ENTIRE JAPAN COASTLINES

R. Jalali Farahani[1], J. Woessner [2], S. Bingi [3], M. Masuda [1]

[1] *Model Development, Risk Management Solutions Inc, Newark, CA, USA, rozita.farahani@rms.com*
[2] *Model Development, Risk Management Solutions Inc, Zurich, Switzerland*
[3] *Model Development, Risk Management Solutions Inc, Noida, India*

Abstract

Probabilistic tsunami hazard assessments are crucial for assessing the hazards imposed on the coastal communities and the results help the decision-makers apply well-informed risk mitigation activities. Seismic sources close to the coastlines can generate large tsunami waves that cause devastating damage and causalities due to the lack of sufficient evacuation time. Thus, the tsunami waves generated from the near-field seismic sources are the main contributors of the tsunami risk. In this study, we have conducted a probabilistic tsunami hazard assessment for the entire Japan coastlines, considering earthquakes modeled on subduction zones off the eastern coast of Japan and within the Japanese sea based on the geometries of the 2017 Japanese seismic hazard model. Stochastic events with non-uniform slip distributions and various magnitudes are generated on each seismic source and triangular dislocation model is used to determine the land/ocean dislocation which serves as the initial condition for the tsunami wave model. Nonlinear shallow water equations are then used to model the tsunami wave propagation and coastal inundations. Inundation hazard maps are provided at cityward and 50m^2 resolution for both eastern and western Japanese coastlines. The exceedance probabilities of the tsunami inundation at different locations along the Japan coastline are provided and we identify the main sources of tsunami hazard at any given region. The results highlight the complexity of inundation height patterns due to tsunami wave incidence direction, coastal processes, earthquake source characteristics as well as complex bathymetry and topographic conditions at the various recurrence intervals. The outputs of this study can be used for general tsunami risk assessment, for tsunami mitigation and risk reduction planning, for tsunami portfolio risk diversification, and tsunami warning system planning.

Keywords: tsunamis, probabilistic hazard analysis, numerical modeling, wave propagation, coastal inundation

1. Introduction

Large tsunami events occur less frequently than other hazards. Yet they can be highly destructive and cause enormous numbers of casualties and economic losses. The limited number of historical records make it difficult to use an accurate empirical hazard assessment and the scenario-based analysis do not cover the risk of all possible events. Recently, Probabilistic Tsunami Hazard Analysis (PTHA) has been developed to quantify tsunami risk and is increasingly used as basis for crucial risk management decisions. PTHA provides information of tsunami hazard at return periods from tens to thousands of years, beyond the limited historical observational data.

Destructive tsunami events are often generated by submarine earthquakes ([1], [2]). Earthquake-generated PTHA methodologies have been introduced in various regions of the world (such as: [3], [4]). Among these studies, most of them have been conducted on coarse resolutions to map tsunami-wave heights, runup and inundation depth, including global-scale and regional-scale grids. However, accurate tsunami risk assessment requires high-resolution calculations since the hazard can change drastically in the scale of tens of meters. The recent huge computational innovations in the field of parallel computations enable us to apply PTHA on high-resolution scales.

In this study, we conducted a PTHA to quantify tsunami hazard (inundation depths) for the entire coastlines of Japan on the high-resolution grids of 50 m^2. We used the 2017 Japanese seismic model (J-SHIS, http://www.j-shis.bosai.go.jp/en/) as basis to identify the tsunamigenic seismic sources and then calculated a stochastic set with non-uniform slip distributions for each source. The seismic characteristics of the sources and the stochastic slip distributions are used to calculate the sea-surface and land deformation including uplift and subsidence. We then modeled the wave propagations and coastal inundations using a numerical model that solves the Non-linear Shallow Water Equations (NLSWE). Finally, we prepared the return period hazard maps for inundated areas along the entire Japan coastlines using two approaches. For the first approach, we aggregated the return period hazard maps to the city ward boundaries. This approach provides valuable risk information at the city ward level [5]. However, a more accurate tsunami risk assessment based on our results can be derived at much higher resolution. Therefore, in the second approach, we prepared the return period hazard maps as well as hazard curves at the 50 m^2 resolution. The results show complex inundation height patterns that change drastically within few tens of meters due to the tsunami wave direction, wave reflection, refraction, and other coastal processes as well as the complex coastal topographic and bathymetric profiles.

2. Model Methodology

2.1 Source Zone Definition and Stochastic Slip Model

To identify the tsunamigenic seismic sources, we selected a subset of stochastic earthquake set modified from the sources contributing to the 2017 National Seismic Hazard Map. This subset includes all offshore events with magnitudes MW≥7.5. We assume that each source in this subset can generate a tsunami that causes substantial losses. Figure 1 shows the locations of the tsunamigenic sources that are used in this study.
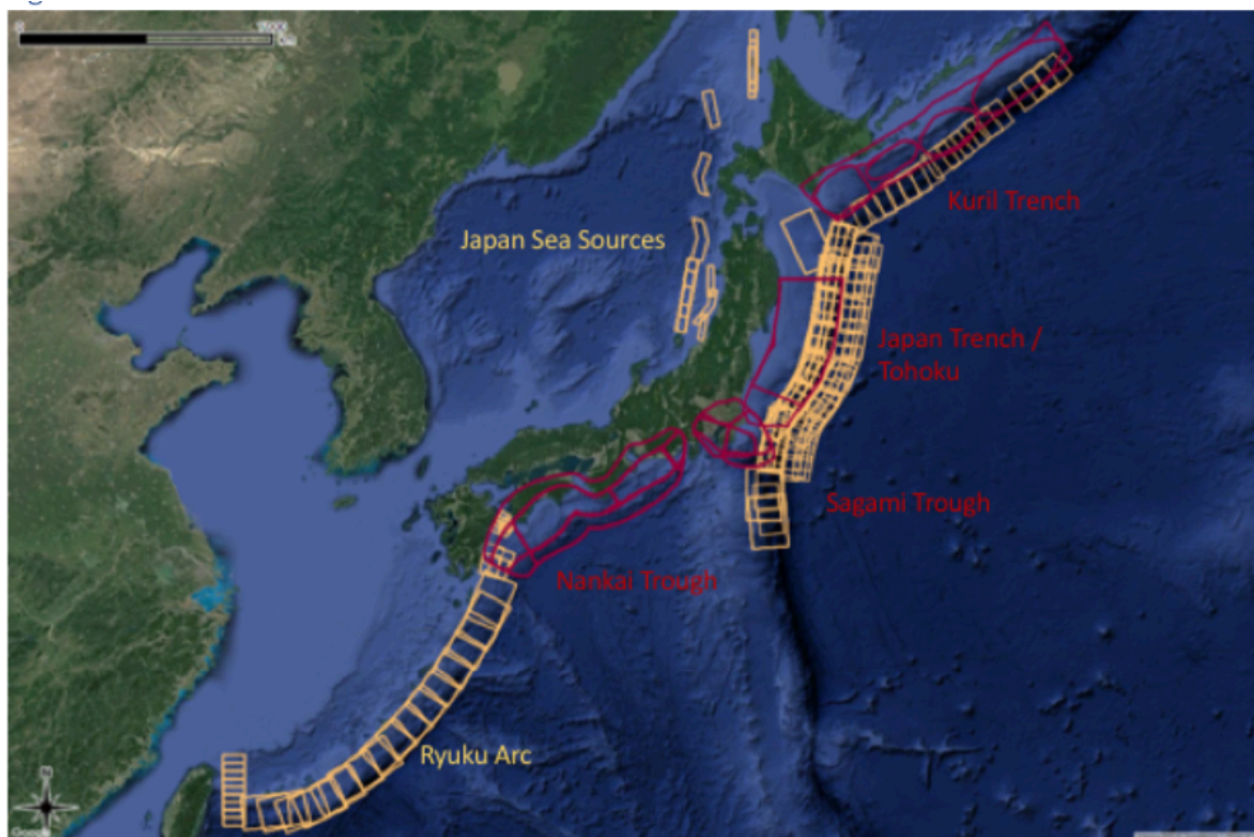
Figure 1 Location of tsunamigenic sources for the Japan local PTHA model. Colors differentiate large subduction interface events (red) and other offshore events that are assumed to generate tsunamis (yellow) based on the 2017 Japanese Seismic Hazard Model.

Recent studies have shown that fault geometry and details of the slip distribution have significant impact on initial tsunami wave heights as well as subsidence or uplift at the coastlines. Consequently, this will have an important impact on the final run-up and inundation depths along the coastal areas ([6], [7], [8], [9], [10], [11]). We generated a stochastic set of slip distributions for each source following the approach proposed by [10]. The selected slip distributions are constrained by a set of criteria including maximum slip, maximum deformation both at the ocean and the coastlines, and location of the slip on the rupture plane. A detailed description of the slip model is included in [12].

2.2 Seafloor/Land Deformation

For every slip distribution generated in the previous section, we computed the seafloor and land deformation following the triangular dislocation model of [13], [14]. The triangular dislocation model presents gap-free parameterizations of complex fault surfaces and avoid the singularities that happen at the edge of dislocation elements when using a rectangular dislocation model. We discretized the seismic sources by Delaunay triangles and applied a dislocation loop where the deformation fields for each of the three triangle legs are calculated by superposing two angular dislocations. Finally, we superposed the deformation of all triangles covering the seismic source to find the seafloor and land deformation fields for each event in the stochastic set. In terms of computational coding, we started with the open-source python codes available by [15] and made them parallel using the Graphics Processing Unit (GPU) parallel computations. This helped us overcome the extensive computational efforts required to model the entire coastlines of Japan. We then used the resulting deformation fields to adjust the ocean bathymetry and land topography after the earthquake occurrences. The deformation fields at the ocean generate the initial tsunami waves, which are input data for the wave model component.

2.3 Wave propagation and coastal inundation

Hydrodynamic characteristics of tsunami waves and the resulting coastal inundations are influenced by several factors including: the initial tsunami waveforms generated in the ocean, the surrounding ocean bathymetric profiles, coastal processes such as wave reflection, wave diffraction, wave refraction, edge waves, land topographic profiles, and land friction coefficients. To accurately model the variations of tsunami height and length during wave propagation and coastal inundation, we solved the Nonlinear Shallow Water Equations (NLSWE) using finite volume numerical method. Since tsunami wavelengths are much larger than the ocean depth, tsunami waves are considered shallow-water waves. Therefore, tsunami wave propagation as well as tsunami runup/inundation can be adequately modelled by the depth integrated NLSWE in the case of non-breaking waves [16]. The HLL approximate Riemann solver is used for the computation of inviscid flux functions [17], [18]. The numerical model is capable to model water flows over a wet or dry bed with complicated boundaries. To accelerate the comprehensive computational efforts, GPU parallel computation was implemented.

We used three levels of nested grids with different resolutions to perform the numerical modeling and capture the coastal processes including wave reflection, diffraction, and refraction: Great Japan Grid of relatively coarse (~1km) resolution (Low resolution grid), 15 grids of intermediate (~450m) resolution (intermediate grid), and 118 grids of fine (~50m) resolution (High resolution grid). The great Japan grid (low resolution grid) of ~1km grid is derived from GEBCO, 2014 gridded bathymetric data sets that include global terrain models for ocean and land [19]. 15 grids of intermediate (~450m) resolution and 118 grids of fine (~50m) resolution are resampled from Japan Cabinet Office elevation data. The grids and the model output of wave elevations are referenced to mean sea level.

We adjusted the bathymetric/topographic computational grids in each of the stochastic tsunamigeneric earthquake events to account for the seafloor/land deformation. The low resolution, intermediate, and high-resolution grids interact with each other by passing boundary conditions between nodes along the intersecting boundaries. At the grid boundaries, wave heights as well as wave fluxes in horizontal directions (x and y) are used as the boundary conditions. The low-resolution grid passes data to the intermediate grids and the intermediate grids pass data to the high-resolution grids. As the wave travels to shallower water, the resolution of grids become finer to accurately model the shorter wavelengths. For all the grids, both land and ocean are considered in the numerical simulations to account for the complicated wave dynamics, refraction, diffraction, wave reflection, and other coastal processes.

3

The initial sea surface displacement at the time of tsunami generation (initial tsunami wave) is assumed to be identical to the seafloor deformation. To incorporate land friction in the hydrodynamic modeling of wave run-up and coastal inundation, we considered variable surface roughness in the wave model. The existence of vegetation or man-made structures alerts the amount and pattern of tsunami inundation. Therefore, it is important to consider the variable surface roughness based on the land cover data. For this purpose, Global Land Use Land Cover (LULC) is used and resampled for the fine resolution grids. For the intermediate grids the roughness data provided by Cabinet office is used. For each stochastic event, we ran the numerical model for 6 hours after the generation of the tsunami waves to model the full lifetime of tsunami waves, coastal processes, and coastal inundation.

3. Tsunami Hazard Results

The PTHA results are presented either as hazard curves or as hazard maps. The hazard curve for a given location presents the annual probability of exceedance as a function of hazard value (For instance: inundation depth or runup). Hazard maps present either the return periods corresponding to exceeding a fixed hazard value or the hazard values corresponding to a fixed annual probability within a geographical area. Both hazard curves and hazard maps provide crucial information for the hazard risk analysis.

We performed PTHA for the entire Japan coastline using the methodology explained in section 2. Then we developed probabilistic tsunami return period maps for the Japan coastlines as well as hazard curves using two approaches. In the first approach, we calculated the maximum inundation depth (I_{max}) and the mean inundation depth (I_{mean}) from all grid cells within a city ward and all tsunami sources. The mean inundation depth (I_{mean}) across a city ward represents an average inundation depth. The maximum inundation depth (I_{max}) results depict a worst-case measurement within a city ward. Figures 2 and 3 illustrate the return period hazard maps for I_{max} and I_{mean} greater than 0.5m, 1m, 5m, and 10m. As shown in these figures, the eastern coastlines of Japan and most of the western coastlines are vulnerable to the inundation depth greater than 0.5m. For inundation depths greater than 1m, 5m, and 10m, eastern coastlines facing Kuril Trench, Japanese trench, Sagami trough, and Nankai trough are more vulnerable to tsunami hazard in comparison to the western coastlines facing the Sea of Japan. For I_{max} and I_{mean} greater than 5m and 10m, the regions facing the Nankai trough have shorter return periods (higher tsunami hazard). Among the coastal city wards facing the Nankai trough, the ones that are closer to the ocean display much higher tsunami hazard specially for the I_{max} greater than 5m and 10m (figure 2). As we travel inland, the complexity of the coastal profiles prevents the tsunami waves and the tsunami hazard decreases. Western Japan coastlines have large return periods (small tsunami hazard) for I_{max} greater than 5m and there is almost no probability for them to get I_{max} greater than 10m. For a given city ward, return periods corresponding to the I_{max} are smaller than the ones corresponding to the I_{mean} as they present the worst-case measurements.

Hazard curves presenting annual probability of exceedance for different maximum inundation depths at six city wards along eastern and western Japan coastlines are shown in figure 4. These city wards include Miyagino-ku Sendai-shi, Isumi-shi, Tateyama-shi, Konohana-ku Osaka-shi, Muroto-shi at the eastern coastlines and Tsuruoka-shi at the western coastlines. Osaka-shi is located further inland as compared to the other five city wards and it is protected by the coastline configuration. Therefore, it presents the lowest maximum inundation depth among these six city wards. On the other hand, Muroto owns the highest maximum inundation depth among these city wards. The annual probability of exceedance corresponding to the 20m maximum inundation depth at this city ward is around 0.02. Isuma-shi also reach a maximum inundation depth of 20m but its corresponding annual probability of exceedance is much less around 0.000001. Sendai-shi has a maximum inundation depth of 11m with an annual probability of exceedance of 0.0006. Tateyama-shi displays larger hazard for maximum inundation depth up to 5m compared to Sendai-shi and Isumi-shi, however, for values above 5m the exceedance probabilities drop substantially below the curves of the two others. Tsuruoka-shi, which is located at the western coastlines, displays lower hazard in comparison to the other eastern cities for maximum inundation depth up to 2m, however for values above 2m it exceeds Osaka-shi as well as Tateyama-shi for maximum inundation depth between 5m to 8m. The results show that even though the western Japan coastlines are much less vulnerable to the tsunami than the eastern coastlines their

4

tsunami hazard should not be ignored. The tsunami waves generated closer to the eastern coastlines can travel far distances and impact the western coastlines as well.
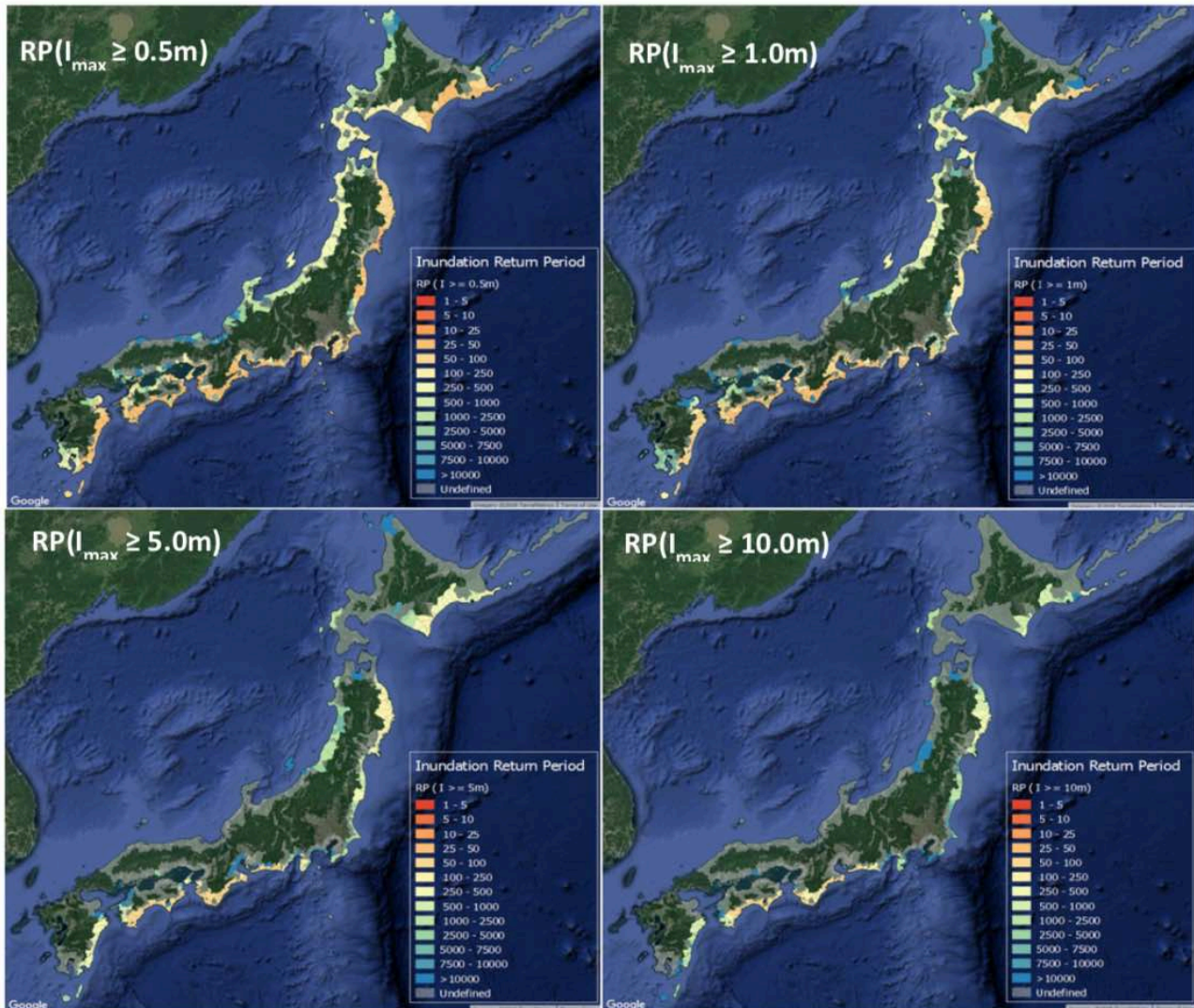
Figure 2 Return period hazard maps aggregated to city ward boundaries for maximum inundation depth (I_{max}) greater than 0.5m, 1m, 5m, 10m

The approach explained in the previous paragraph provides valuable information on the tsunami hazard at the city ward level and can be used in the risk mitigation practices. However, tsunami is a high-resolution hazard and the inundation depths can vary drastically in adjacent regions due to a variety of factors including change of coastline profile, topography elevation, land friction coefficient, surrounding bathymetry, wave direction, etc. Therefore, the approach explained above can result in overestimation and/or underestimation of tsunami hazard in a city ward because a single value of maximum inundation depth (I_{max}) or the mean inundation depth (I_{mean}) is considered to present risk for the entire city ward. For that reason, we took a second approach to develop probabilistic tsunami return period maps and hazard curves at the 50 m^2 resolution grids instead of city ward polygons. We developed these high-resolution hazard maps and hazard curves for the entire eastern and western Japan coastlines. In this paper we focus on the Sendai and Ishinomaki regions as they were the most vulnerable regions during the historical 2010 tsunami event and unfortunately a large number of people passed away in these regions.

5
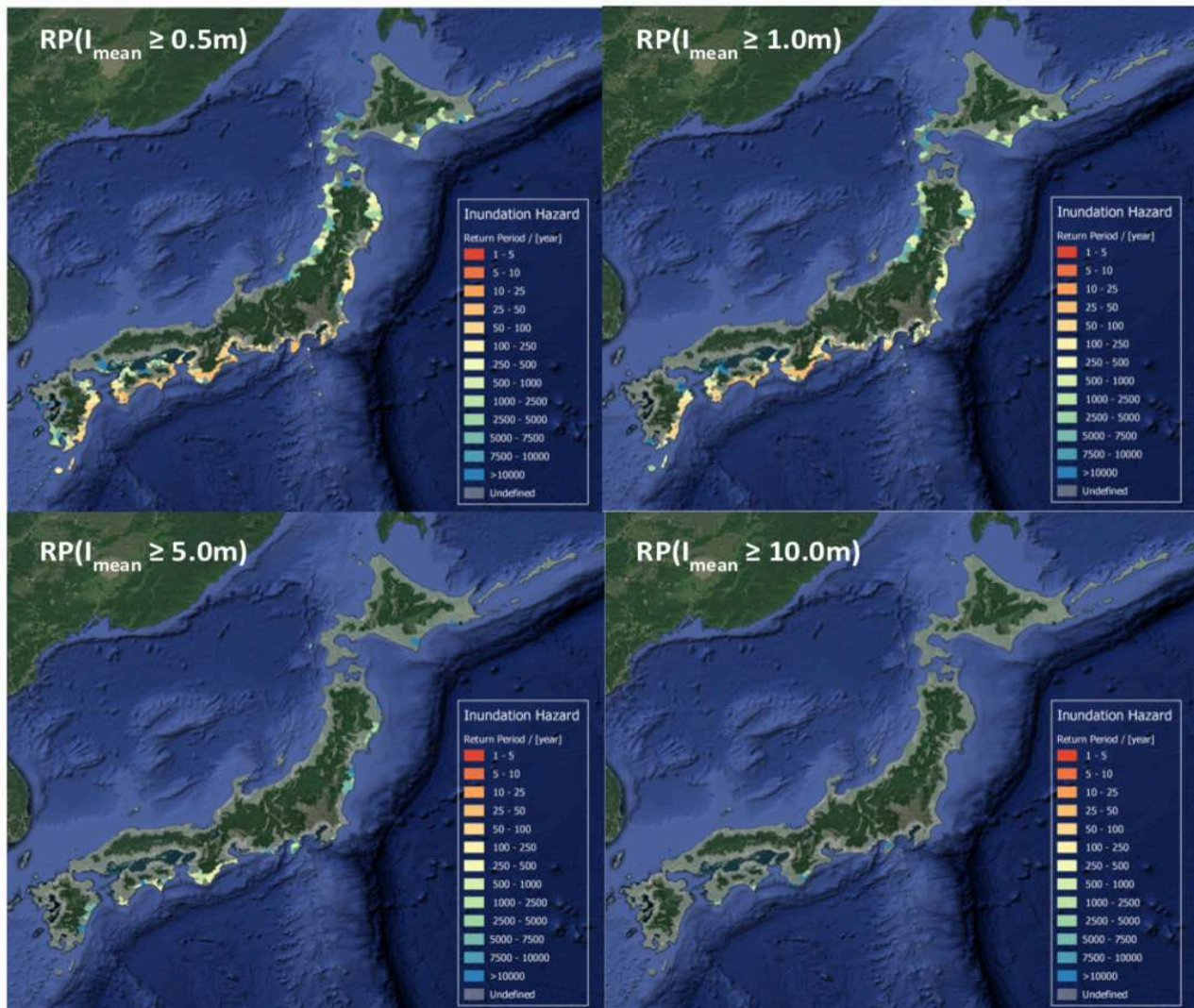
Figure 3 Return period hazard maps aggregated to city ward boundaries for mean inundation depth (I_{mean}) greater than 0.5m, 1m, 5m, 10m

Figure 5 shows the return period hazard maps for inundation depth greater than 1m, 5m, and 10m at the Sendai and Ishinomaki regions. The entire coastline in these regions are vulnerable to tsunami inundation greater than 1m. As we go inland from the coastline, the return periods increase as the tsunami inundations decrease due to the higher elevation and/or the impact of the land friction resistance. A large number of grid cells that are located immediately close to the coastline get an inundation depth of at least 1m for a return period of 100-250 years. Most of the coastlines in this region are also vulnerable to the inundation depth greater than 5m. A small portion of cells immediately close to the coastlines can get inundation depth greater than 10m. Complex return period patterns can be observed in the adjacent cells along the coastline. For instance, Higashimatsushima gets high tsunami inundation hazard except a small portion at the west. The western part of Higashimatsushima as well as Matsushima get much lower tsunami hazard as the coastline configuration protects these regions from the tsunami waves. Ishinomaki gets high tsunami inundation hazard except some regions at the east. High elevation values at the eastern part of Ishinomaki prevent the tsunami waves to travel inland. In addition, the tsunami wave directions and coastal processes such as wave reflection, wave refraction

6
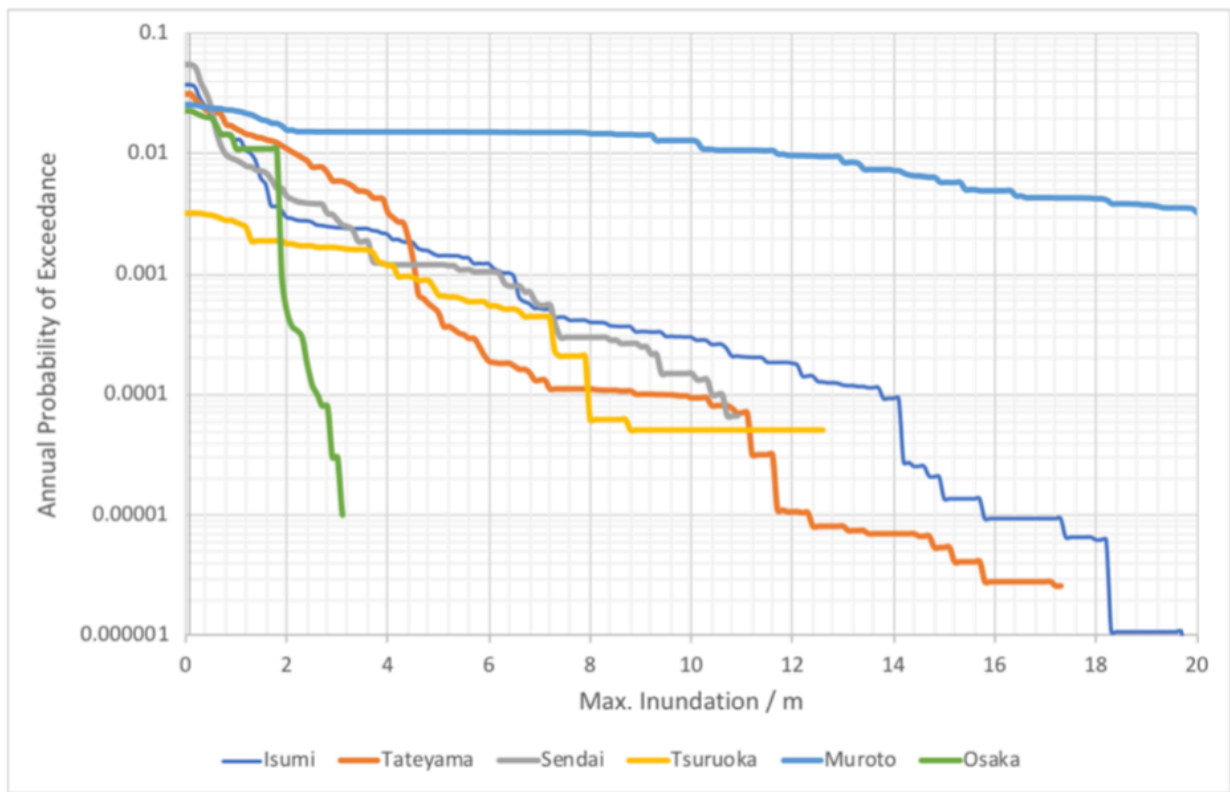
Figure 4 Annual probability of Exceedance for maximum inundation depth at six Japan coastal cities: Sendai-shi, Isumi-shi, Tateyama-shi, Osaka-shi, Muroto-shi at the eastern coastlines and Tsuruoka-shi at the western coastlines

7

, edge waves play an important role on the tsunami hazard maps and can only be modeled at the high-resolution scale. If we look at the hazard maps at the city ward scale (figure 2 and 3), we see that one value of maximum inundation and one value of mean inundation are assigned to the entire city ward. For instance, the entire Ishinomaki gets maximum inundation depth (I_{max}), greater than 1m for return period of ~100 years and based on the mean inundation depth (I_{mean}), Ishinomaki gets no tsunami inundation depth greater than 1m. However, if we look at Ishinomaki in figure 5, we see a much more detailed pattern of return period values at varying locations that can only be identified at the high-resolution scale. We conclude that the first approach (city ward scale) gives overestimation and/or underestimation of the tsunami hazard and the second approach (high resolution) displays more accurate and detailed results.

We created hazard curves illustrating annual probabilities of exceedance for tsunami inundation depths along the western and eastern Japan coastlines. Here we are presenting the hazard curves at 6 locations in Ishinomaki and Higashimatsushima regions. Figure 6 shows these hazard curves. Point 1 and Point 2 are both located at the western part of Higashimatsushima but they have very different tsunami risk. Point 1 is protected by the coastal configuration and gets a maximum inundation depth of ~4m with an annual probability of exceedance equal to 0.0001. Point 2 gets an inundation depth of ~20m with the same annual probability of exceedance equal to 0.0001. Point 3 and point 4 are not far in distance but point 4 is further inland so the tsunami hazard is much less at point 4 in comparison to the point 3. Annual probability of exceeding 2m inundation depth for point 3 is ~0.003, while the same annual probability of exceedance for point 4 is ~0.00003. Point 5 is located at Onagawa and point 6 is located at the eastern part of Ishinomaki. Point 5 shows larger tsunami risk for inundation depth up to 5m. From inundation depth 5 to 12m, point 5 and 6 show very similar trends. However, for values above 12 m, point 6 shows larger tsunami risk. For inundation depth equal to 20m, both point 5 and point 6 get the same annual exceedance probability of ~0.00003. Various behaviors in terms of annual probability of exceedances for different inundation depths can be observed in adjacent regions as tsunami hazard can vary drastically in couple of meters at the various recurrence intervals.
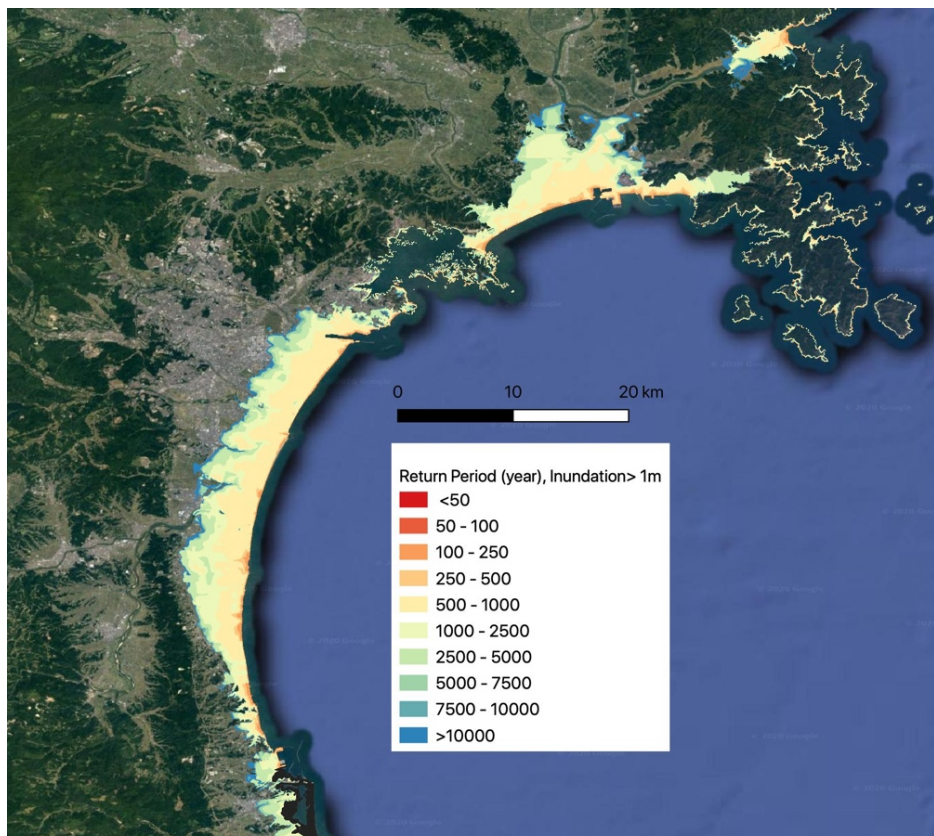
Figure 5 Return period hazard maps provided at 50 m^2 resolution for inundation depth greater than 1m, 5m, 10m

8
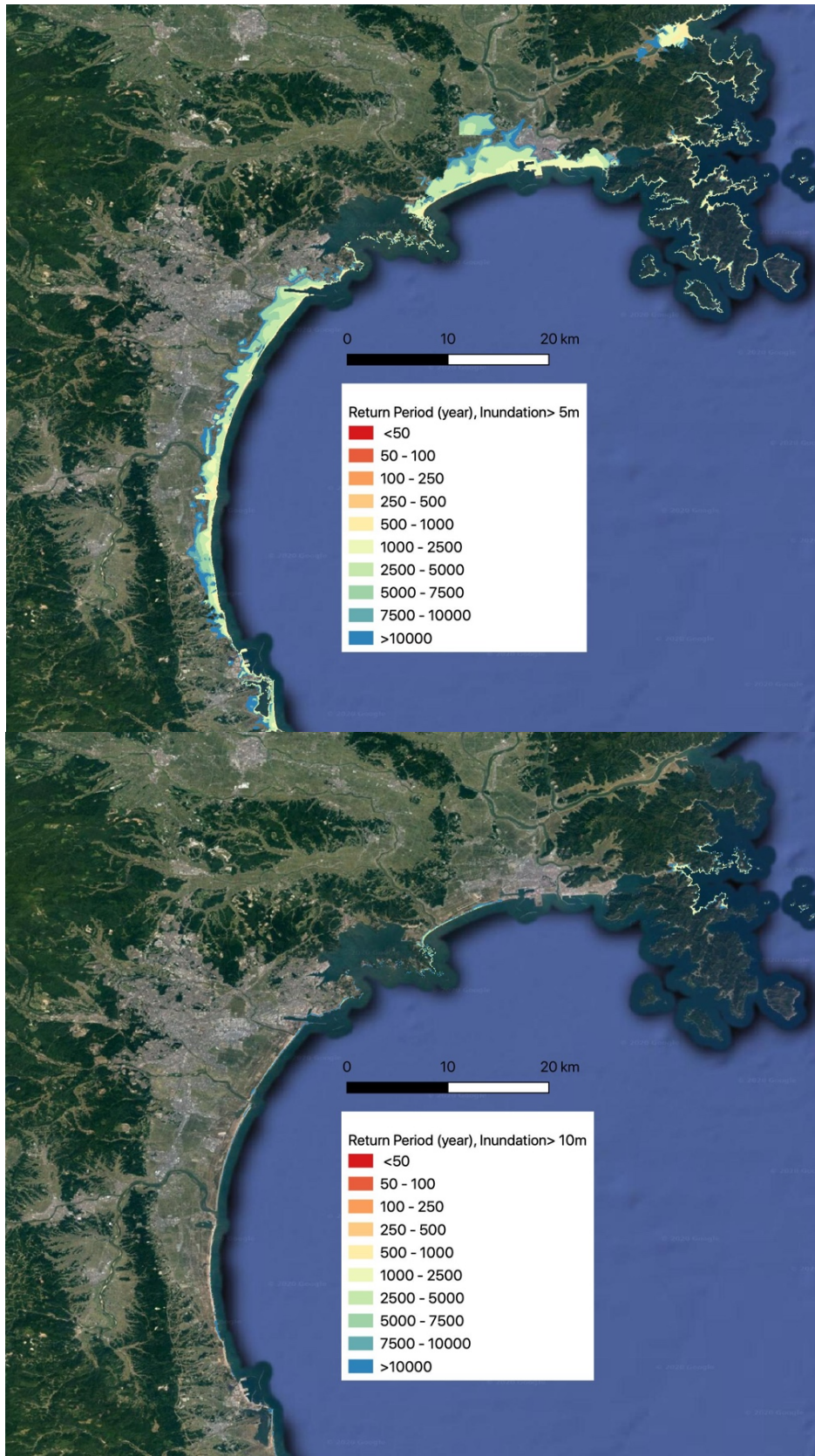
Figure 5 (Continued) Return period hazard maps provided at 50 m^2 resolution for inundation depth greater than 1m, 5m, 10m

9
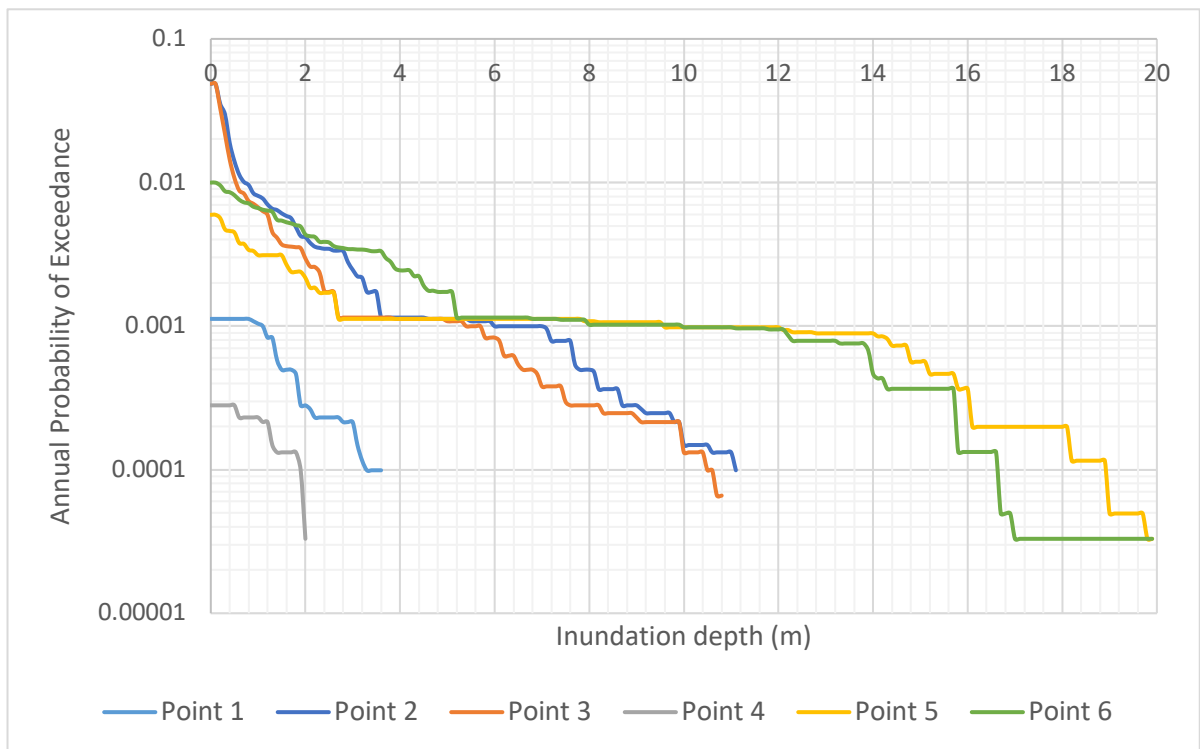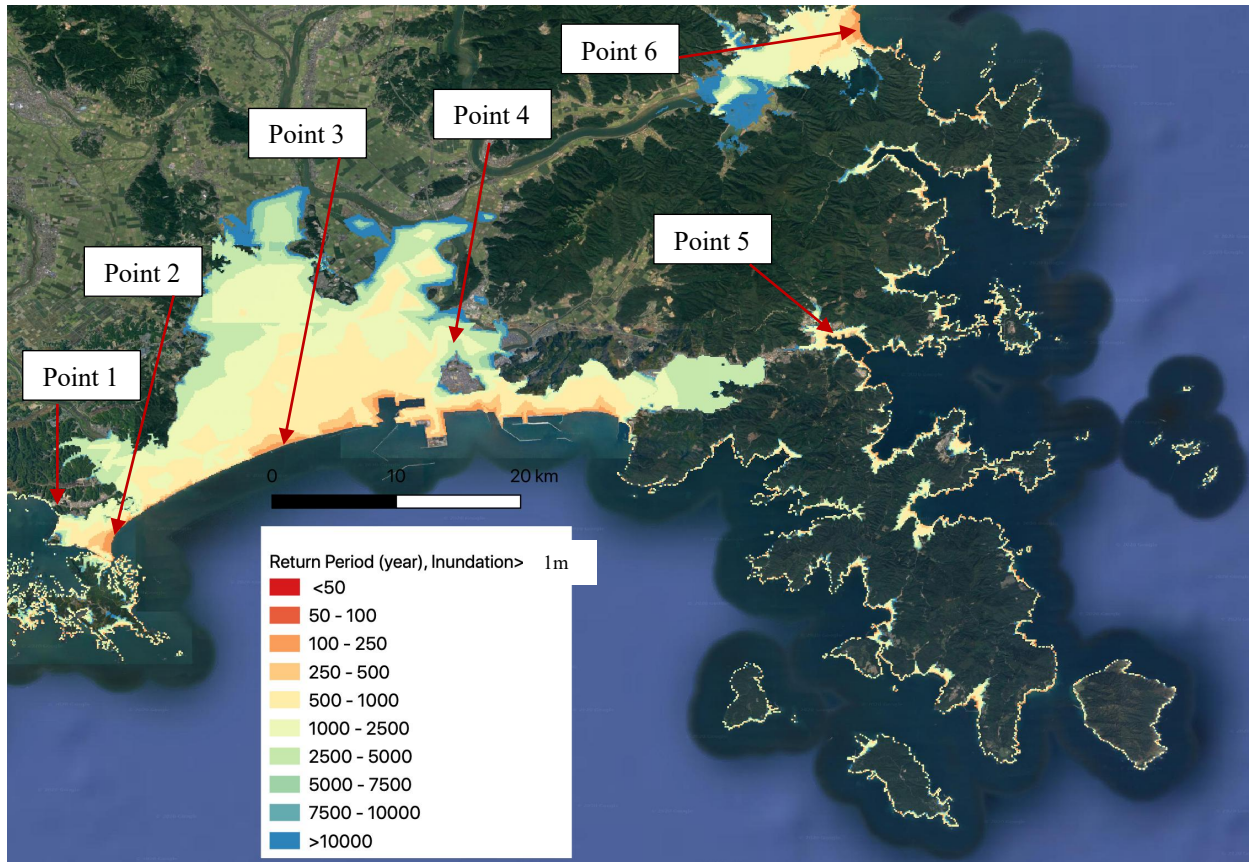
Figure 6 Annual probability of exceedance for tsunami inundation at 6 locations in Ishinomaki and Higashimatsushima regions

10

4. Conclusions

Quantifying tsunami inundation hazard at various resolutions is an essential input to tsunami risk assessment. In this study we show that tsunami hazard is highly variable depending on the selected resolution and that it is useful and adequate for different purposes to display tsunami hazard at various scales. Paramount to this process is an initial high-resolution solution that enables to identify small scale variations in tsunami hazard. This is extremely valuable for local scale measure, such as planning evacuation routes or identifying location level risk of particular buildings. However, on a coarser scale, it is also informative to map tsunami hazard on administrative regions such as city wards for country-wide risk assessment.

Our study is among the first studies that addresses probabilistic tsunami hazard on a national scale for Japan. Our source model and rate model are based on the Japanese Seismic Hazard Model 2017, with some modifications to single sources and rates ([21]). We created a stochastic set of slip distributions for each earthquake source and applied detailed deformation model and numerical wave model to obtain tsunami coastal inundations at 50 m^2 grid cells. The underlying risk model is not comprehensive as roughly 750 tsunamis generating stochastic events underly the results and particularly the short return period hazard is probably under sampled. However, it is one of the first nationwide results providing essential information on hazard relativities and details especially along the eastern coast. We presented the tsunami return period hazard maps and hazard curves using two approaches: (1): Hazard aggregation to to the city ward scale: we calculated the maximum inundation depth (I_{max}) and the mean inundation depth (I_{mean}) from all grid cells within a city ward and all tsunami sources. (2): High-resolution 50 m^2 scale: we calculated the hazard curves and hazard maps at 50 m^2 grid cells. Our results show that the high-resolution approach gives more accurate and detailed understanding of the tsunami risk at the various recurrence intervals. We found the highest tsunami risk along the eastern coastlines specifically along the south-eastern coastlines. However, the tsunami risk along the western coastlines cannot be neglected. Detailed high-resolution tsunami returns period maps and hazard curves are provided for Sendai and Ishinomaki regions. Results show various return period patterns and hazard curves exceedance probabilities at adjacent regions and emphasize the importance of the high-resolution detailed modeling.

5. References

[1] Grezio A, et al. (2017): Probabilistic Tsunami Hazard Analysis: Multiple Sources and Global Applications. *Reviews of Geophysics*, 1-41. https://doi.org/10.1002/2017RG000579

[2] Satake K, Atwater B F, (2007): Long-term perspectives on giant earthquakes and tsunamis at subduction zone. *Annual Review of Earth and Planetary Sciences*, **35**, 349-74. https://doi.org/10.1146/annurev.earth.35.031306.140302

[3] Davies G, et al. (2017): A Global probabilistic tsunami hazard assessment from earthquake sources. *Geological Society, London, Special Publications*, 219-244. https://doi.org/10.1144/SP456.5

[4] Geist E L, Parsons T (2006): Probabilistic analysis of tsunami hazards. *Natural Hazards*, **37**, 277-314. https://doi.org/10.1007/s11069-005-4646-z

[5] Woessner J, Farahani R J, (2020): Tsunami inundation hazard across Japan, *International Journal of Risk Reduction*, in review

[6] Davies G, et al. (2015): Tsunami inundation from the heterogeneous earthquake slip distributions: Evaluation of synthetic models. Journal of Geophysical Research: Solid Earth, **120** (9), 6431-6451. https://doi.org/10.1002/2015JB012272

[7] Goda K, et al. (2014): Sensitivity of tsunami wave profiles and inundation simulations to earthquake slip and fault geometry for the 2011 Tohoku earthquake. *Earth, Planets and Space*, **66** (1), 105. https://doi.org/10.1186/1880-5981-66-105

11

[8] Horspool N, et al. (2014): A probabilistic tsunami hazard assessment for Indonesia. *Natural Hazards and Earth System Science*, **14** (11), 3105-3122. https://doi.org/10.5194/nhess-14-3105-2014

[9] LeVeque R J, et al. (2016): Generating Random Earthquake Events for Probabilistic Tsunami Hazard Assessment. *Pure and Applied Geophysics*. https://doi.org/10.1007/s00024-016-1357-1

[10] Melgar D, et al. (2016): Kinematic rupture scenarios and synthetic displacement data: An example application to the Cascadia subduction zone. *Journal of Geophysical Research: Solid Earth*. https://doi.org/10.1002/2016JB013314

[11] Selva J, et al. (2016): Quantification of source uncertainties in Seismic Probabilistic Tsunami Hazard Analysis (SPTHA). *Geophysical Journal International*, **205** (3), 1780-1803. https://doi.org/10.1093/gji/ggw107

[12] Woessner J, et al. (2018): Tsunami risk for insurance portfolios in Japan. *16th European Conference on Earthquake Engineering,* Thessaloniki, Greece.

[13] Meade B J, (2007): Algorithms for the calculation of exact displacements, strains, and stresses for triangular dislocation elements in a uniform elastic half space. *Computers & Geosciences*, **33** (8), 1064-1075. https://doi.org/10.1016/j.cageo.2006.12.003

[14] Nikkhoo M, Walter T R, (2015): Triangular dislocation: an analytical, artefact-free solution, *Geophys. J. Int.*, **201,** 1119–1141. https://doi.org/10.1093/gji/ggv035

[15] Styron R, (2019): tri_dislocations_python, Zenodo, https://github.com/cossatot/tri_dislocations_python, DOI: 10.5281/zenodo.3368513

[16] Pedersen G, Lovholt F, (2008): Documentation of a global Boussinesq solver, *Mechanics and Applied Mathematics*, **1**, 1–69. https://www.duo.uio.no/handle/10852/10184.

[17] Yoon T H, Kang S K, (2004): Finite Volume Model for Two-Dimensional Shallow Water Flows on Unstructured Grids, *J. Hydraul. Eng*, **130**, 678–688. doi:10.1061/(ASCE)0733-9429(2004)130:7(678).

[18] Zhu F, Dodd N, (2018): Riemann solution for a class of morphodynamic shallow water dam- break problems, *J. Fluid Mech*., **835**, 1022–1047. doi:10.1017/jfm.2017.794.

[19] Sandwell D T, et al. (2002): Bathymetry from Space: Oceonography, Geophysics and Climate, *Geoscience Professional Services*, Maryland, https://www.geo-prose.com/pdfs/bathy_from_space.pdf.

[20] Simons M, et al. (2011): The Tohoku-ki Earthquake: Mosaicking the Megathrust from seconds to centuries. *Science*, **332**, 1421-1425.

[21] Fitzenz D D, (2018): Conditional Probability of What? Example of the Nankai Interface in Japan. *Bulletin of the Seismological Society of America,* **108** (6), 3169-3179.